

DEPARTMENT OF
ATMOSPHERIC SCIENCES



OREGON
STATE
UNIVERSITY

Strand Agriculture Hall 326
Corvallis, Oregon
97331-2209

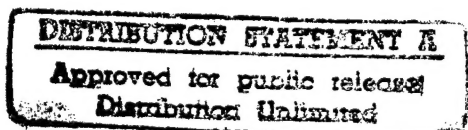
Dr. R.F. Abbey, Jr.
Director, Marine Meteorology Research
Office of Naval Research
Code 1122 MM
800 Quincy Street
Arlington, VA 22217

14 June, 1995

ONR Grant # N00014 - 90 - J - 1480
OSU Account # 30 - 262 - 3111

Dear Bob:

In order to complete my ONR grant entitled "Satellite Observations of Marine Stratus/Stratocumulus," I am sending three copies of the *Final Technical Report* to you with copies distributed as indicated.



Sincerely,

A handwritten signature in ink, appearing to read "Jim Coakley".

James A. Coakley, Jr.

cc: Defense Technical Information Center (2 copies)
Bldg. 5, Cameron Station
Alexandria, VA 22304-6145

Administrative Contracting Officer (1 copy)
Office of Naval Research
Seattle Regional Office
1107 NE 45th Street, Suite 350
Seattle, WA 98105-4631

Director, Naval Research Laboratory (1 Copy)
Attn: Code 2627
Washington DC 20375

Telephone
503-737-4557

Fax
503-737-2540

Omnet
OREGON.ST.ATMOS

Telex
510 496 0682 OSU COVS

DTIC QUALITY INSPECTED 5

19970717 163



DEPARTMENT OF THE NAVY
OFFICE OF NAVAL RESEARCH
SEATTLE REGIONAL OFFICE
1107 NE 45TH STREET, SUITE 350
SEATTLE WA 98105-4631

IN REPLY REFER TO:

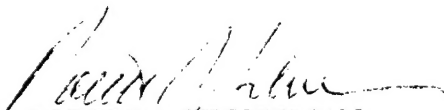
4330
ONR 247
11 Jul 97

From: Director, Office of Naval Research, Seattle Regional Office, 1107 NE 45th St., Suite 350, Seattle, WA 98105
To: Defense Technical Center, Attn: P. Mawby, 8725 John J. Kingman Rd., Suite 0944, Ft. Belvoir, VA 22060-6218

Subj: RETURNED GRANTEE/CONTRACTOR TECHNICAL REPORTS

1. This confirms our conversations of 27 Feb 97 and 11 Jul 97. Enclosed are a number of technical reports which were returned to our agency for lack of clear distribution availability statement. This confirms that all reports are unclassified and are "APPROVED FOR PUBLIC RELEASE" with no restrictions.

2. Please contact me if you require additional information. My e-mail is silverr@onr.navy.mil and my phone is (206) 625-3196.


ROBERT J. SILVERMAN

FINAL TECHNICAL REPORT

ONR GRANT # N00014 - 90 - J - 1480

James A. Coakley, Jr.
College of Oceanic and Atmospheric Sciences
Oregon State University
Corvallis, OR 97331-2209

Satellite Observations of Marine Stratus/Stratocumulus

ABSTRACT

Work supported by this ONR Grant led to the stream lining of spatial coherence analysis software and allowed the application of the spatial coherence analysis to a large volume of satellite imagery data. The analyses were performed in order to obtain the properties of low-level clouds and the cloud-free ocean background. The work led to the findings that: 1) reflectivities of broken clouds at both 0.63 and 3.7 μm are smaller than those of nearby uniform clouds indicating that the broken clouds have substantially less liquid water than do their uniform counterparts and that photons are escaping through the sides of the broken clouds and being absorbed by the ocean surface. 2) The thin atmosphere approximation used to justify the split window technique for obtaining sea surface temperatures from satellite imagery data fails to give the sensitivity of the emitted radiances to variations in the atmospheric optical path that arise from changes in the scan angle of the imaging radiometer. 3) Substantial portions of low-level marine stratocumulus are semitransparent at 11- μm . 4) As do fractional cloud cover and liquid water amount, droplet radius appears to vary from pixel to pixel at the scale available from conventional satellite imagery data (1 km). 5) Comparisons of cloud cover derived using the spatial coherence method applied to satellite imagery data for the Atlantic Stratocumulus Transition Experiment (ASTEX) with cloud cover predicted by forecast models indicated that the forecast models were unable to adequately predict low-level clouds. The deficiency was thought to be due to the inability of the model to adequately predict the relative humidities in the upper levels of the boundary layer.

LIST OF PUBLICATIONS SUPPORTED BY THIS ONR GRANT

Bretherton, C.S., E. Klinker, A.K. Betts and J.A. Coakley, Jr., 1995: Comparison of ceilometer, satellite and synoptic measurements of boundary layer cloudiness and the ECMWF diagnostic cloud parameterization scheme during ASTEX. *J. Atmos. Sci.* (in press).

Kowalski, A. S., 1992: Satellite Infrared Measurement of Sea Surface Temperature: Empirically Evaluating the Thin Approximation. M.S. Thesis. College of Oceanic and Atmospheric Sciences, Oregon State University.

Luo, G., X. Lin, and J.A. Coakley, Jr., 1994: 11- μm emissivities and droplet radii for marine stratocumulus, *J. Geophys. Res.*, **99**, 3685-3698.

1. Introduction

The goal of this project was to develop automated procedures incorporating the spatial coherence method for analyzing cloud properties from satellite imagery data and then to use the analysis scheme to analyze the cloud properties obtained during the Atlantic Stratocumulus Transition Experiment (ASTEX). ASTEX took place in the Northeastern Atlantic in June 1992. During the course of the project, the spatial coherence analysis software was streamlined and large volumes of satellite imagery data were analyzed. The analyzed results afforded opportunities to characterize the properties of marine stratocumulus and to test the assumptions underlying the estimation of sea surface temperatures (SSTs) from multispectral infrared imagery data. Also, a new approach was developed for analyzing cloud properties from multispectral infrared imagery data. The new approach provided a test of the opaque cloud approximation used in the spatial coherence method to obtain the fractional cloud cover for imager pixels ($\sim 1 - 4$ km) that are only partly cloud covered. The new approach itself was subjected to consistency checks with the 1-km Advanced Very High Resolution Radiometer (AVHRR) data collected during ASTEX. Finally, the cloud cover derived from the ASTEX observations using the spatial coherence method was used to assess the performance of cloud parameterization schemes used in weather forecast models. These various projects and their findings are described in the following sections.

2. Reflectivities of Uniform and Broken Layered Cloud Systems

The spatial coherence method was used to obtain cloud properties for ASTEX. It was applied to the 1-km AVHRR data collected by the Naval Post Graduate School during the experiment. The special feature of the spatial coherence method is that it distinguishes between imager pixels that are cloud-free, overcast, and partly cloud-covered. Following an earlier study (Coakley, 1991), the data collected during ASTEX was analyzed to obtain the reflectivities

of low-level, layered cloud systems at 0.63 and 3.7 μm . Reflectivities of low-level clouds that completely covered several of the 1-km pixels were obtained along with the reflectivities of clouds that only partly covered the 1-km pixel. The spatial coherence results were used to segregate overcast pixels from partly cloudy pixels. Comparisons were made between the reflectivities for the overcast and broken clouds within localized (~ 60 km) regions so that the properties of the uniform and broken clouds were arguably identical save for their different extents cloud cover.

Figure 1 shows the reflectivities of low-level, layered clouds at 0.63 and 3.7 μm derived from the overcast pixels (solid curves) and differences in the reflectivities (overcast – broken) (dashed curves) obtained for the nearby partly cloudy pixels collected during ASTEX. The observations are for the afternoon passes of the NOAA-11 satellite. The reflectivities are presented as functions of satellite zenith angle. Positive zenith angles indicate radiation that is reflected in the direction of forward scattering; negative zenith angles indicate radiation that is reflected in the direction of backward scattering. Points indicate mean values and error bars indicate the expected uncertainty (one standard deviation) in the mean values. The uncertainty is estimated on the basis of the variability of the observations obtained during ASTEX.

Like the results reported by Coakley and Judge (1991) for a set of pre-ASTEX observations, the ASTEX observations conform to the findings reported by Coakley (1991). At the visible wavelength, broken clouds have lower reflectivities than their uniform counterparts. As with the earlier study, the discount factor is approximately 0.8. This reduction is due either to smaller column amounts of cloud liquid water in the broken clouds or to the escape of photons from the sides of the broken clouds and their subsequent absorption by the ocean surface. Regardless of the mechanism, the anisotropy of the radiation reflected by broken clouds is, within the uncertainty of the observations, similar to that reflected by uniform clouds.

At 3.7 μm , reflectivities of broken clouds are smaller than those of their uniform counterparts for radiation that is reflected in the direction of backward scattering (indicated by negative satellite zenith angles) and larger than the reflectivities of their uniform counterparts for radiation that is reflected in the direction of forward scattering (indicated by positive satellite zenith angles). The higher reflectivities for broken clouds in the forward scattering direction should, however, be viewed with caution. At 3.7 μm , cloud-free oceans exhibited large reflectivities (not shown), even larger than those for overcast pixels. The high reflectivities correspond with high reflectivities at 0.63 μm and are evidently due to sunglint. Because of the sunglint, estimates of reflectivities for clouds that only partly cover the pixels may be subject to large errors. Differences in the reflectivities for the radiation reflected in the direction of backward scattering, however, are reliable. As with the reflectivities at visible wavelengths, the reduction in reflectivities for the broken clouds can be explained either due to a decrease in the amount of cloud water for broken clouds or to the escape of photons from the sides of the clouds. Unlike the reflectivities at visible wavelengths, however, the anisotropy of 3.7- μm radiation reflected by broken clouds would appear to differ from that reflected by uniform clouds. Radiation reflected by broken clouds would be more isotropic than that reflected by uniform clouds.

3. SSTs from AVHRR Observations

The spatial coherence analysis was applied to 4-km AVHRR observations for the months of May, June, and July 1983 and 1984 to determine the types of cloud conditions that were likely to be found during ASTEX. In addition to the information on cloud properties, these observations provided opportunities to test concepts commonly used for retrieving sea surface temperatures (SSTs) from 11 and 12- μm imagery data. As part of the work undertaken under

this ONR grant, Mr. A. Kowalski completed the requirements for an MS degree in Atmospheric Sciences at OSU.

Kowalski explored the possibility of inferring SSTs from the relationships exhibited by the emitted radiances themselves, i.e. without the need to obtain collocated buoy or shipboard measurements of SSTs (Kowalski, 1993). The approach was based on the analysis of the split-window technique for obtaining SSTs given by McMillin (1975) and by McMillin and Crosby (1984). According to McMillin, the radiance observed in channel 4 (11 μm) of the AVHRR should be linearly related to the difference in the radiances observed in channels 4 and 5 (12 μm). The relationship is given by

$$I_4 = B_4(T_s) + \gamma (I_4 - I_5') \quad (1)$$

where $B_4(T_s)$ is the Planck function at the surface temperature T_s , which is the desired SST, γ is a constant, and I_5' is the radiance in channel 4 that would be observed if the observed channel 5 brightness temperature were used to calculate the channel 4 radiance. Usually, γ is determined by correlating (1) with *in situ* buoy or shipboard observations of T_s . The form of (1), however, suggests that if a region has a sufficiently uniform surface temperature so that $B_4(T_s)$ is constant, then γ is the slope for the relationship between I_4 and $I_4 - I_5'$.

Kowalski searched $5^\circ \times 5^\circ$ latitude – longitude regions containing numerous cloud-free pixels as determined by spatial coherence analysis of 4-km AVHRR observations for May-July 1983 and 1984 in the north Atlantic ($5^\circ\text{N} - 45^\circ\text{N}$, $10^\circ\text{W} - 40^\circ\text{W}$). Few regions were found in which a linear relationship between I_4 and $I_4 - I_5'$ could be claimed. The lack of linear relationships was probably caused by sea surface temperature gradients within the ~ 500 km regions. The analysis of smaller regions was impractical because significant variations of I_4 and $I_4 - I_5'$ across the region are needed in order to obtain a reliable estimate of γ . If the SST is

uniform across the region, variations of I_4 and $I_4 - I_5'$ are due to changes in the atmospheric optical path which come with changes in satellite zenith angle (i.e. with changes in the scan angle of the AVHRR).

Figure 2 shows one incident in which a relationship in accordance with (1) was observed. In this case $\gamma = -4.8$. The commonly used value is $\gamma \sim -3$. The magnitude of γ increases as the burden of water vapor in the atmosphere increases.

The lack of regions with sufficient uniformity in SST to obtain values of γ was surprising and led to the assessment of the "thin atmosphere" approximation that gives rise to (1). Using a radiative transfer model for the emitted radiances observed by the AVHRR, Kowalski calculated radiances as a function of satellite zenith angle for tropical, midlatitude and polar profiles of temperature and moisture. The results are shown in Figure 3. The figure demonstrates that (1) is unsuitable for changes in the radiance due to the changes in the optical path that come with changes in satellite zenith angle. Owing to the nonlinear relationship between the emitted radiances and the column amount of water vapor, the slopes obtained on the basis of changes in the radiances with satellite zenith angle (dashed lines) are grossly biased values of γ (solid lines) for tropical and midlatitude profiles. The slope is a useful estimate only in the case of a polar profile, which has little water vapor, and consequently, is appropriate for the "thin atmosphere" approximation.

4. Retrieval of Cloud Properties from Multi-Spectral Infrared Imagery Data

Clouds, particularly low-level maritime clouds, cannot be expected to fill the field of view of a radiometer having even a 1-km resolution. Broken clouds within a field of view should be the norm. Clouds, on the other hand, usually come in well-defined layers. By finding

geographically localized regions ($\sim 4 - 8$ km) of uniform emission, the spatial coherence method utilizes the tendency of clouds to form layers to identify pixels which are overcast by layered clouds. The localized geographic regions which lack uniform emission are presumed to contain broken clouds. In order to obtain the fractional cloud cover of regions with broken clouds, the assumption is made that the clouds within the region being analyzed are opaque and part of the layer, or layers, indicated by the localized regions exhibiting uniform emission. Through NASA support for the FIRE project, Lin and Coakley (1993) developed a new approach for obtaining the properties of layered cloud systems from imagery at two infrared wavelengths. Work supported in part through this ONR grant used the Lin and Coakley retrieval scheme to characterize the properties of marine stratocumulus off the coast of Chile (Luo et al., 1994). Work also supported in part through this ONR grant extended the Lin and Coakley retrieval scheme to determine whether there was consistency in the retrievals when all five channels of the AVHRR were utilized (Coakley and Lin, 1993).

For single-layered cloud systems, the emitted radiance observed by channel i of a satellite radiometer is given by

$$I_i = (1 - A_c)I_{si} + A_c(\epsilon_i I_{ci} + t_i I_{si}), \quad (2)$$

where I_{si} is the radiance associated with the cloud-free portion of the pixel, ϵ_i is the average emissivity of the clouds in the pixel at the wavelengths associated with channel i , I_{ci} is the emission that would be observed if the pixels were overcast by the clouds and if the clouds were black at the wavelengths associated with channel i and t_i is the average transmissivity of the clouds. Here it is assumed that the observations are being made in an atmospheric "window" so that emission by the atmospheric gases above the clouds is taken to be negligible. As is illustrated in Figure 4, based on (2), emitted radiances from two distinct spectral intervals, (e.g., 11 and 12 μm or 3.7 and 12 μm) are constrained to fill the radiance domain bracketed by well-prescribed

limits. If the clouds are opaque, then $t_i = 0$ and $\epsilon_i = \epsilon_{iMAX}$ where $\epsilon_{iMAX} = 1 - r_{iMAX}$ and r_{iMAX} is the maximum value of the reflectivity that can be obtained at the wavelengths associated with channel i . At some wavelengths where absorption is appreciable, like at 11 and 12 μm , r_{iMAX} may be taken to be zero. According to (2) when the clouds are part of a single layer and they are opaque at any two thermal infrared wavelengths, then the radiances at these wavelengths are linearly related. Such relationships have often been observed at night for 3.7 and 11- μm radiances (Coakley and Davies, 1986). For pixels that are overcast by single-layered clouds that are semitransparent at the infrared wavelengths associated with one or both channels, then again according to (2), the radiances will be nonlinearly related through the separate nonlinear dependencies of emissivity and transmissivity on the optical path length. Finally, for pixels that are overcast by clouds that are opaque for any two infrared channels and are distributed in altitude, the radiances will follow, aside from effects due to absorption and emission in the cloud-free atmosphere, the Planck blackbody curve.

Using various values of A_c in (2) along with various values for the liquid/ice water column amounts for droplets with a fixed size distribution to calculate values of ϵ_i and t_i , a set of curves are generated which may be used to interpret the observed radiances. The curves are shown in Figure 4. For 60 km regions, single-layered cloud systems are often broken. They often have radiative properties which are consistent with a range of optical pathlengths. Consequently, instead of giving rise to radiances that fall along a particular line, whether it be linear or nonlinear, the radiances appear to fill the radiance domain bracketed by the extremes. An example is shown in Figure 5. Cloud cover and optical pathlength (or equivalently, as is given in the figure, the 11- μm emissivity) are then assigned to a pixel-scale radiance pair on the basis of the radiances predicted by the radiative transfer model. The results shown in the figure are obtained using the Eddington approximation to calculate ϵ_i and t_i .

As was noted by Lin and Coakley (1993), the size of the domain covered by the infrared radiances is a function of hydrometeor size. The area covered is generally large for small droplets and collapses to a straight line (no area) for large droplets. Cloud properties are retrieved from radiance pairs by adjusting the effective particle radius (and also the emission associated with opaque, overcast clouds) in the radiative transfer model until the predicted radiance domain tightly hugs the observed radiances (Lin and Coakley, 1993). An example is shown in Fig. 5.

Luo et al. (1993) used 4-km resolution emitted radiances at 11 and 12 μm from the NOAA-9 AVHRR to survey the properties of marine stratocumulus off the coast of South America. They found droplet radii that vary within the typically observed ranges ($\sim 8 - 12 \mu\text{m}$). One of the surprising results of this study was that a substantial fraction of the area covered by marine stratocumulus is semitransparent at 11 μm . The 250 km average 11- μm emissivity was between 0.7 and 0.8. These results were consistent with the earlier findings of Wielicki and Parker (1992). Conventional wisdom took marine stratocumulus to be black. Radiative transfer and aircraft observations had indicated that such clouds become opaque when they reach depths of 100 - 450 m, a common occurrence (Platt, 1976). But during field experiments, thin clouds are often avoided as the mission is generally to obtain the properties of clouds: so, the thicker the cloud the better. As a result, there is abundant evidence from field programs that such clouds are black.

Not only were marine stratocumulus found to be semitransparent, but also their average emissivity was found to be a function of the regional scale cloud cover as is shown in Figure 6. Evidently, if the region is heavily cloud covered, the ratio of semitransparent to opaque cloud material decreases. The consequence is that, not surprisingly, regional scale cloud cover and liquid water column amounts are related to each other.

If this multispectral infrared retrieval procedure is to be believed, then cloud cover, liquid/ice water column amounts and particle size obtained using one set of wavelengths, e.g. 11 and 12 μm should match those obtained using a second set, e.g. 3.7 and 12 μm (Coakley and Lin 1993). There should be a one-to-one mapping of the pixels in the two-channel radiance domains as is illustrated in Figure 7. Figures 8 and 9 show an experiment that tests this mapping. Nighttime observations are used in order to avoid the reflection of sunlight at 3.7 μm . In the test the 11 and 12- μm radiances are used to identify clusters of pixels that would appear to be overcast by semitransparent clouds (squares) and clusters of pixels that would appear to be partly covered by opaque clouds (triangles) (Fig. 8). The location of the pixel clusters in the 3.7-12- μm radiance domain is shown in Fig. 9. Clearly, the interpretation based on the 11-12- μm radiance pairs is inconsistent with that based on the 3.7-12- μm radiance pairs.

Even though only one example is presented, the example is representative of observations for single-layered cloud systems found at night. The same principles were used to test the consistency of emitted radiation at 11 and 12 μm with emitted radiation at 11 μm and reflected sunlight at 0.63 μm . As with emission at 3.7, 11 and 12 μm , the interpretation based on emission at 11 and 12 μm does not hold for observations at 0.63 and 11 μm . The conclusion drawn from the results of these tests is that effective particle size, like fractional cloud cover and cloud optical path, varies from pixel to pixel at the 1-km spatial resolution available to the AVHRR. A simple solution to rectify this inconsistency would be to utilize observations at say, 3.7, 11 and 12 μm to derive fractional cloud cover, particle size and cloud optical path on a pixel by pixel basis. Arking and Childs (1985) proposed such a scheme, albeit using reflected sunlight at 0.63 μm and 3.7 μm and emitted radiances at 11 μm . Work on this problem is continuing through support by NASA.

5. Evaluation of ECMWF Cloud Parameterization Scheme during ASTEX

Spatial coherence analyses of cloud cover and cloud top height (as indicated by the observed 11- μ m brightness temperature for overcast pixels) during ASTEX were compared with surface based estimates of cloud cover from ceilometer data and predictions of cloud cover using ECMWF model forecast and analysis fields combined with various diagnostic cloud parameterization schemes (Bretherton et al., 1995). Cloud properties obtained with the spatial coherence method applied to 1-km AVHRR data were analyzed on a $2^\circ \times 2^\circ$ latitude – longitude grid. At this scale, low-level cloud systems were often accompanied by upper level cloud systems, impeding the analysis of conditions when low-level clouds existed by themselves. Figure 10 shows a comparison of the analyzed satellite derived fractional cloud cover with that inferred for the corresponding three-hour period of ceilometer observations on Porto Santo when only low-level clouds, as deduced from the satellite observations were present. The agreement is satisfying, if somewhat surprising, given the differences in the spatial scales associated with the two different observations. The ceilometer observations are for clouds directly over the site. With the 7 m s^{-1} surface wind observed during ASTEX, the average for the three hour period would seem appropriate for a $\sim 70 \text{ km}$ region downwind of the site. The satellite analysis, on the other hand, is for 200 km scale regions. Nevertheless, high values of the cloud cover in the satellite observations correspond with high values in the ceilometer observations and conversely low values in the satellite observations correspond with low values in the ceilometer observations.

The agreement between satellite and ceilometer based observations is to be contrasted with the lack of agreement between the cloud cover obtained with the ECMWF cloud parameterization scheme and the ceilometer cloud cover shown in Figure 11. The cloud cover predicted using the ECMWF scheme with either the model generated or analyzed fields was too low. The chief deficiency in the model was thought to be the relatively low values of the relative humidity near the top of the boundary layer produced by the model (Bretherton et al., 1995).

6. Summary of Findings

The work supported under this ONR grant led to the following findings:

- Reflectivities at $0.63\ \mu\text{m}$ and $3.7\ \mu\text{m}$ for broken, low-level, layered clouds observed during ASTEX were smaller than the reflectivities of their uniform counterparts. The lower values may be explained by either lower amounts of cloud liquid water in broken clouds or by the escape of photons through the sides of broken clouds.
- The optically thin approximation used to justify split window techniques for the estimation of sea surface temperature from satellite infrared imagery data cannot be used to infer the variation of the emitted radiances with satellite zenith angle. The relationship between the emitted radiances and the atmospheric optical pathlength is nonlinear and outside of the range appropriate for the optically thin approximation to apply.
- A substantial portion of marine stratocumulus resides in cloud material that is semitransparent at $11\ \mu\text{m}$. The average $11\text{-}\mu\text{m}$ cloud emissivity for 250-km scale regions lies between 0.7 and 0.8.
- Like fractional cloud cover and liquid water path, droplet radius for marine stratus appears to vary from pixel to pixel at the highest resolutions available to conventional satellite observations ($\sim 1\ \text{km}$).

- Owing to their inability to predict the high levels of relative humidity which appear to be present in the upper levels of the boundary layer, forecast models are unable to predict the presence of low-level cloud.

References

- Arking A. and J.D. Childs, 1985: The retrieval of cloud cover parameters from multispectral satellite images. *J. Climate Appl. Meteorol.*, **24**, 322-333.
- Bretherton, C.S., E. Klinker, A.K. Betts and J.A. Coakley, Jr., 1995: Comparison of ceilometer, satellite and synoptic measurements of boundary layer cloudiness and the ECMWF diagnostic cloud parameterization scheme during ASTEX. *J. Atmos. Sci.* (in press).
- Coakley J.A., Jr. and R. Davies, 1986: The effect of cloud sides on reflected solar radiation as deduced from satellite observations. *J. Atmos. Sci.*, **42**, 1025-1035.
- Coakley, J.A., Jr., 1991: Reflectivities of uniform and broken layered clouds. *Tellus*, **43B**, 420-433.
- Coakley, J.A., Jr. and D.V. Judge, 1991: Reflectivities of uniform and broken layered clouds. Symposium on Aerosol-Cloud-Climate Interactions, XX IUGG General Assembly, 13-20 August 1991, Vienna.
- Coakley, J.A., Jr., and X. Lin, 1993: Consistency of multiwavelength infrared retrievals for marine stratocumulus, 1993 Spring Meeting, American Geophysical Union
- Kowalski, A. S., 1992: Satellite Infrared Measurement of Sea Surface Temperature: Empirically Evaluating the Thin Approximation. M.S. Thesis. College of Oceanic and Atmospheric Sciences, Oregon State University.
- Lin, X. and J.A. Coakley, Jr., 1993: Retrieval of properties for semitransparent clouds from multispectral infrared imagery data. *J. Geophys. Res.* **98**, 18,501-18,514.
- Luo, G., X. Lin, and J.A. Coakley, Jr., 1994: 11- μ m emissivities and droplet radii for marine stratocumulus, *J. Geophys. Res.*, **99**, 3685-3698.
- McMillin, L.M., 1975: Estimation of sea surface temperatures from two infrared window measurements with different absorption, *J. Geophys. Res.*, **80**, 5113-5117.
- McMillin, L.M. and D.S. Crosby, 1984: Theory and validation of the multiple window sea surface temperature technique, *J. Geophys. Res.*, **89**, 3655-3661.
- Platt, C.M.R., 1976: Infrared absorption and liquid water content in stratocumulus clouds. *Quart. J. R. Met. Soc.*, **102**, 553-561.
- Wielicki, B.A., and L. Parker, 1992: On the determination of cloud cover from satellite sensors: The effect of sensor spatial resolution, *J. Geophys. Res.*, **97**, 12,799-12,823.

Figure Captions

Figure 1. Reflectivities for overcast pixels (solid line) and differences in reflectivities (overcast – broken) at $0.63\ \mu\text{m}$ (a) and $3.7\ \mu\text{m}$ (b) obtained for low-level, layered cloud systems observed during ASTEX. The symbols indicate average values for the indicated satellite zenith angle; the error bars indicate estimates of the uncertainty (one standard deviation) in the mean values. Positive satellite zenith angles indicate the forward scattering direction; negative values indicate the backward scattering direction.

Figure 2. Linear relationship between the observed cloud-free radiance in channel 4 ($11\ \mu\text{m}$), I_4 , of the AVHRR and the difference between the channel 4 radiance and the channel 4 radiance that would be obtained for the channel 5 ($12\ \mu\text{m}$) brightness temperature $I_4 - I_5'$. The observations are for a $5^\circ \times 5^\circ$ latitude – longitude region. The linear relationship is expected if the sea surface temperature is uniform across the region. The variation of I_4 and I_5' across the region is presumed to be due to the variation of optical path with AVHRR scan angle across the region.

Figure 3. Slopes giving γ in (1). Solid lines are the actual values of γ . Dashed lines are the values of γ predicted on the basis of the variations in I_4 and $I_4 - I_5'$ with satellite zenith angle.

Figure 4. 11 and $12\text{-}\mu\text{m}$ radiances given by (2) for a single-layered, low-level cloud system exhibiting various degrees of fractional cloud cover and cloud water path as indicated by the $11\text{-}\mu\text{m}$ emissivities. Solid lines are lines of constant cloud cover with the cloud cover given by the numbers above the lines. Dashed lines are lines of constant $11\text{-}\mu\text{m}$ emissivity with the emissivities given at the ends of the lines. The calculations were performed for a cloud with mean droplet radius, $R_{\text{eff}} = 2.7\ \mu\text{m}$.

Figure 5. Observed and theoretically calculated 11 and 12- μm radiances.

Figure 6. Average cloud cover and 11- μm emissivity for 250-km regions containing low-level marine stratocumulus off the coast of Chile.

Figure 7. Bispectral consistency which should exist if the assumptions underlying the multispectral retrieval procedures are valid.

Figure 8. Identification of pixel clusters containing opaque, broken clouds (triangles) and overcast semitransparent clouds (squares) based on emission at 11 and 12 μm .

Figure 9. Mapping of pixel clusters containing opaque, broken clouds (triangles) and overcast semitransparent cloud (squares) as identified through their emission at 11 and 12 μm . For a consistent mapping, the squares should fall on the upper envelope of the 3.7-12- μm radiance domain occupied by the radiance pairs and the triangles should fall along the straight line.

Figure 10. Spatial coherence estimates of low-level cloud cover and corresponding estimates based on ceilometer observations at Porto Santo during the ASTEX experiment.

Figure 11. ECMWF estimates of low level cloud cover and corresponding estimates based on ceilometer observations at Porto Santo during the ASTEX experiment.

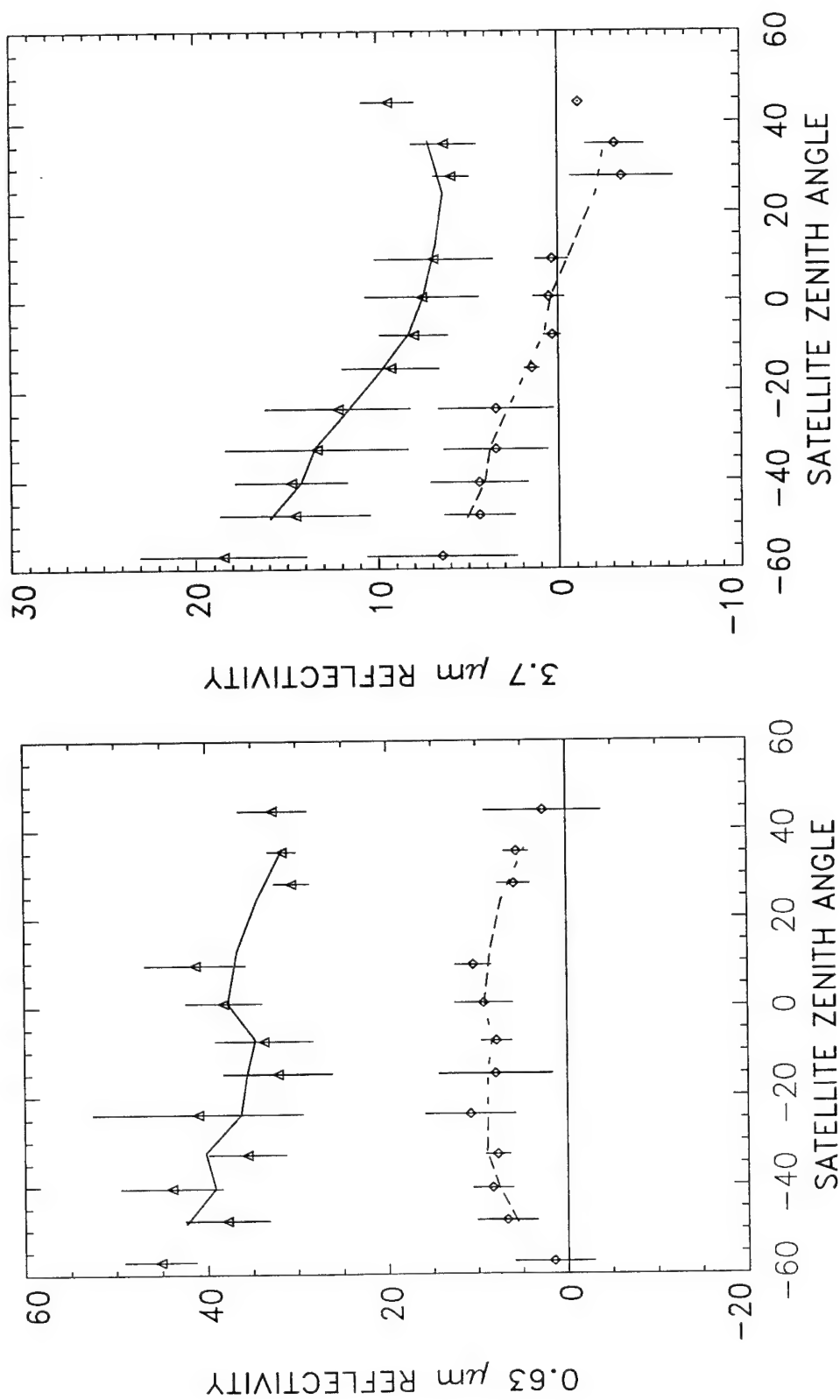


Figure 1

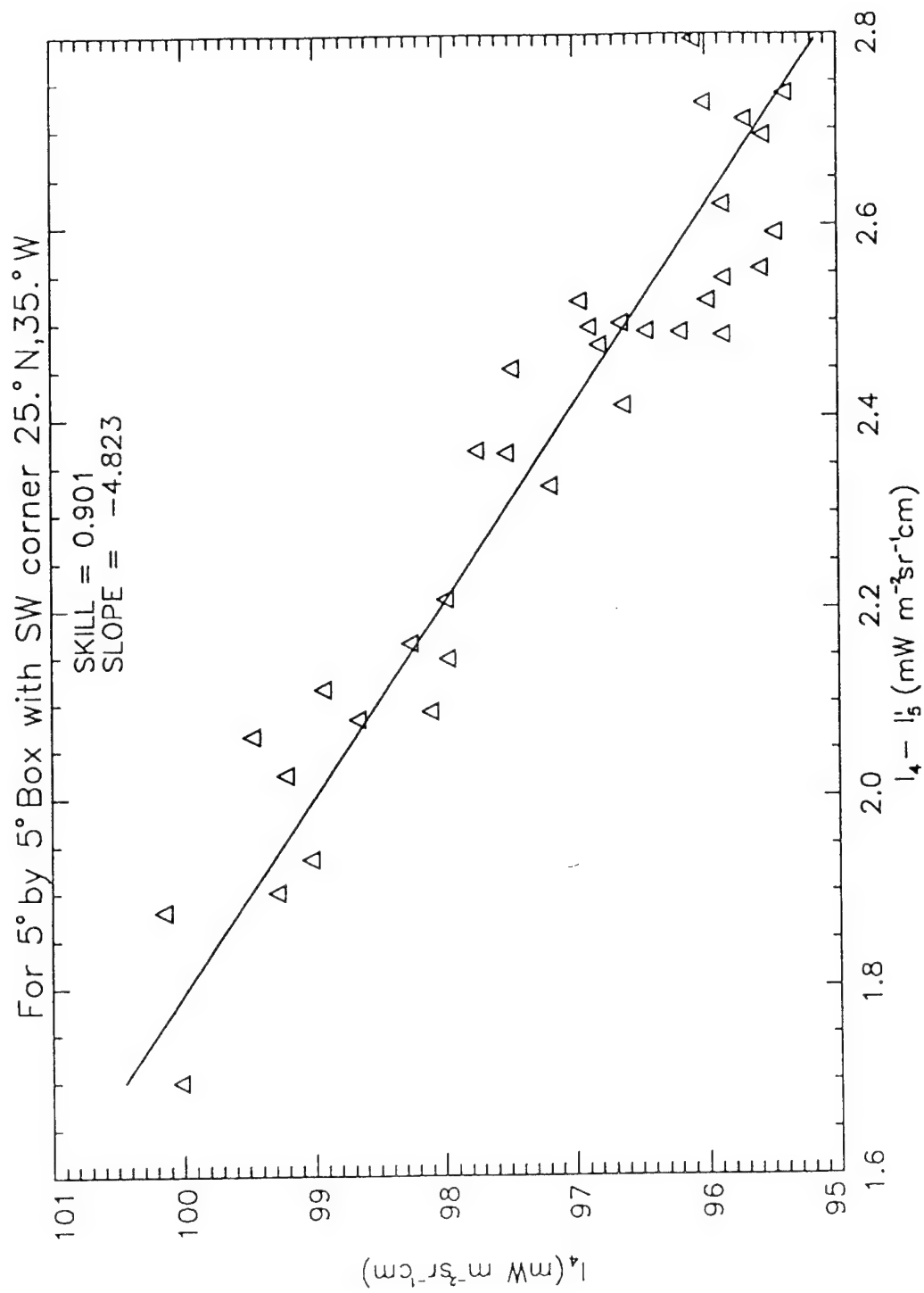


Figure 2

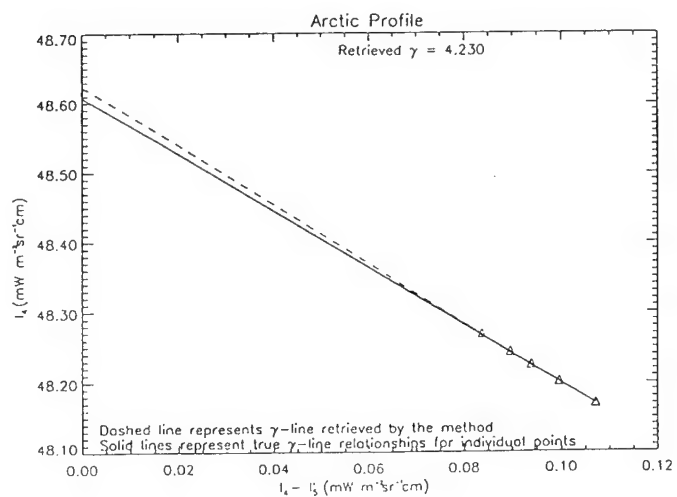
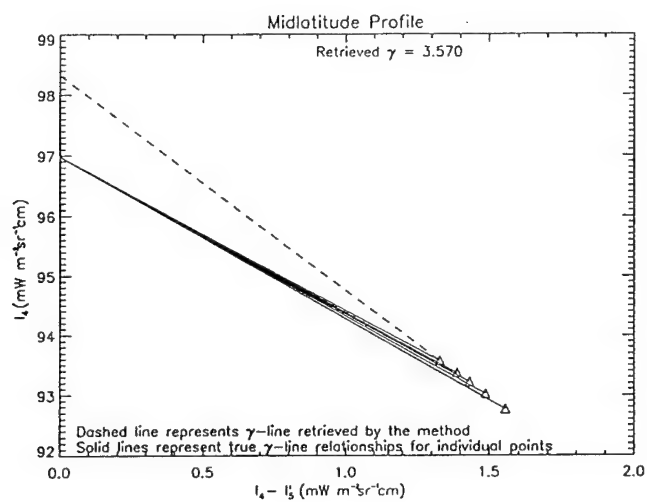
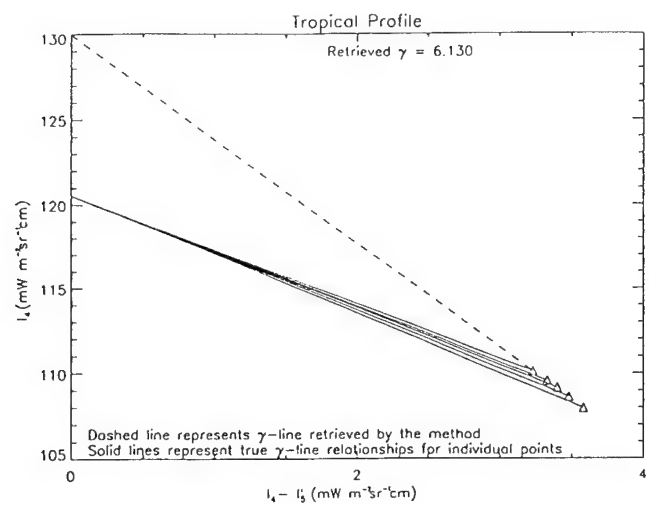
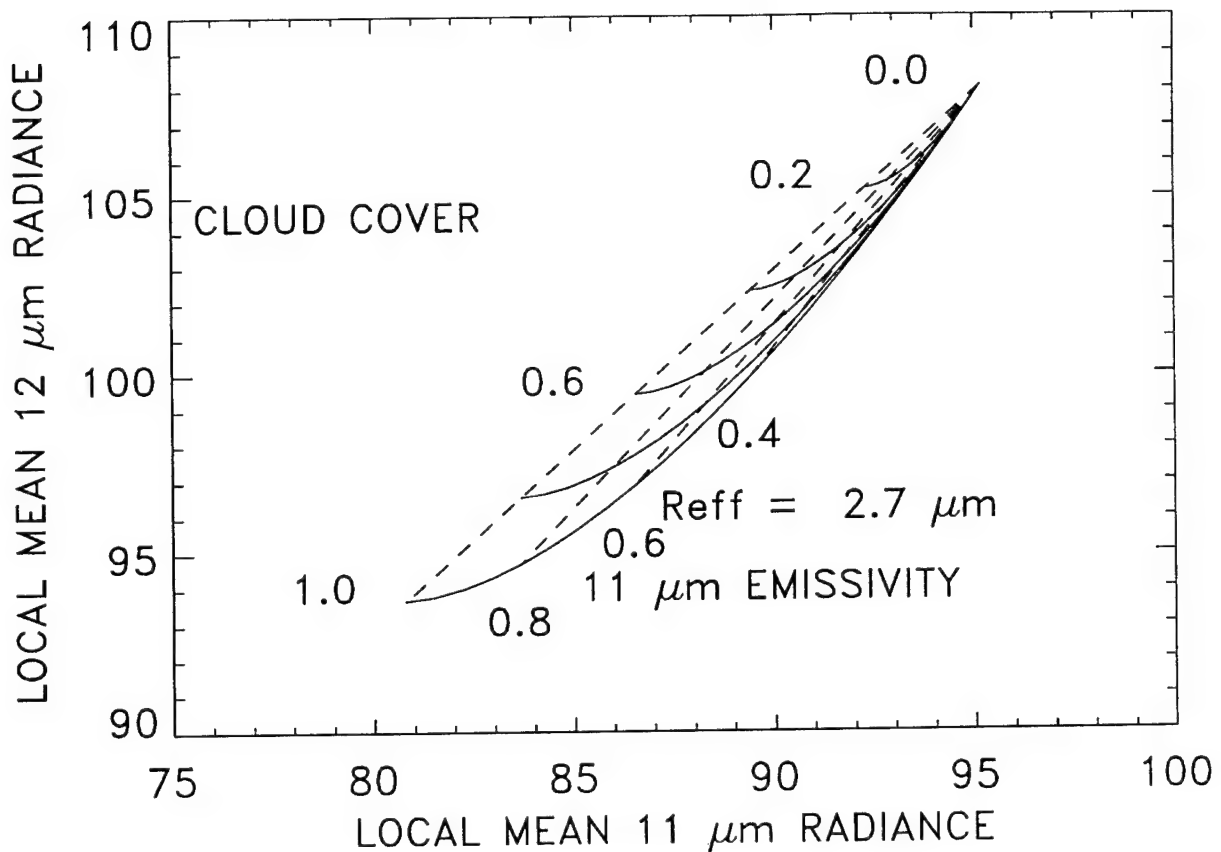


Figure 3

Theory

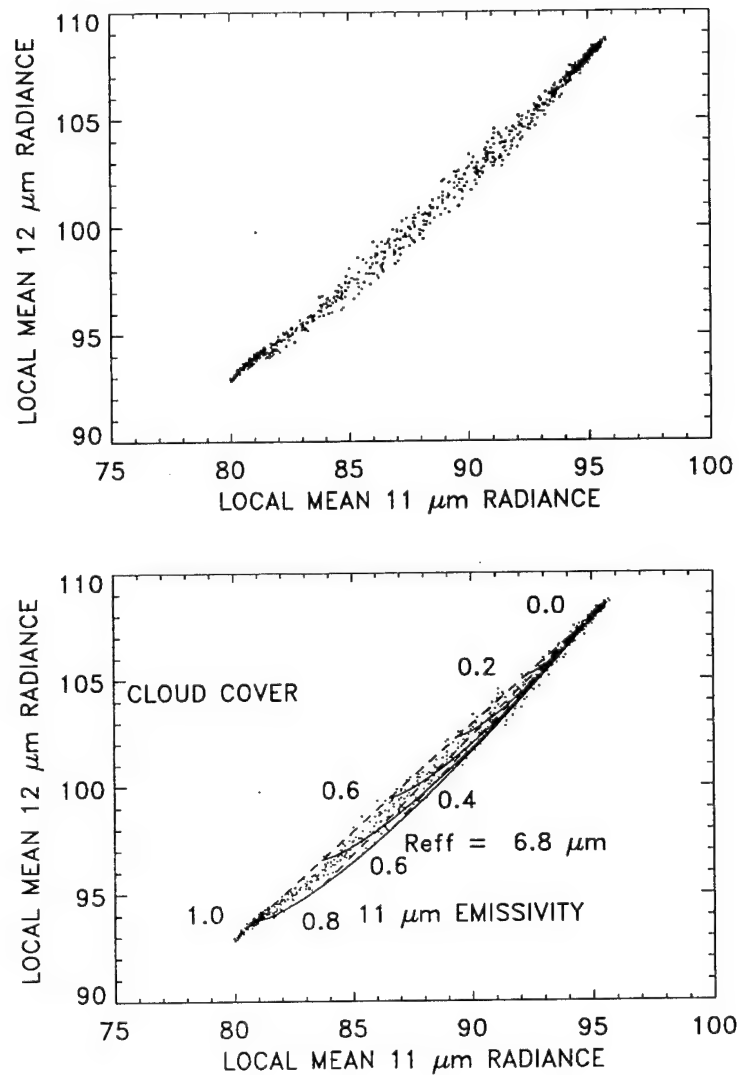
11-12 μm Radiance Pairs



1. Single-Layer, plane-parallel.
2. Eddington approximation.
3. Observed cloud-free and overcast radiances.
4. Homogeneous droplet radii given by log-normal size distribution.

Figure 4

Fit to Observations



2 \times 2 arrays of 1-km HRPT data from nighttime overpass of NOAA-11 for 60-km scale portion of ASTEX region containing single-layered marine stratocumulus system. 10 June 1992, 0412 Z

Figure 5

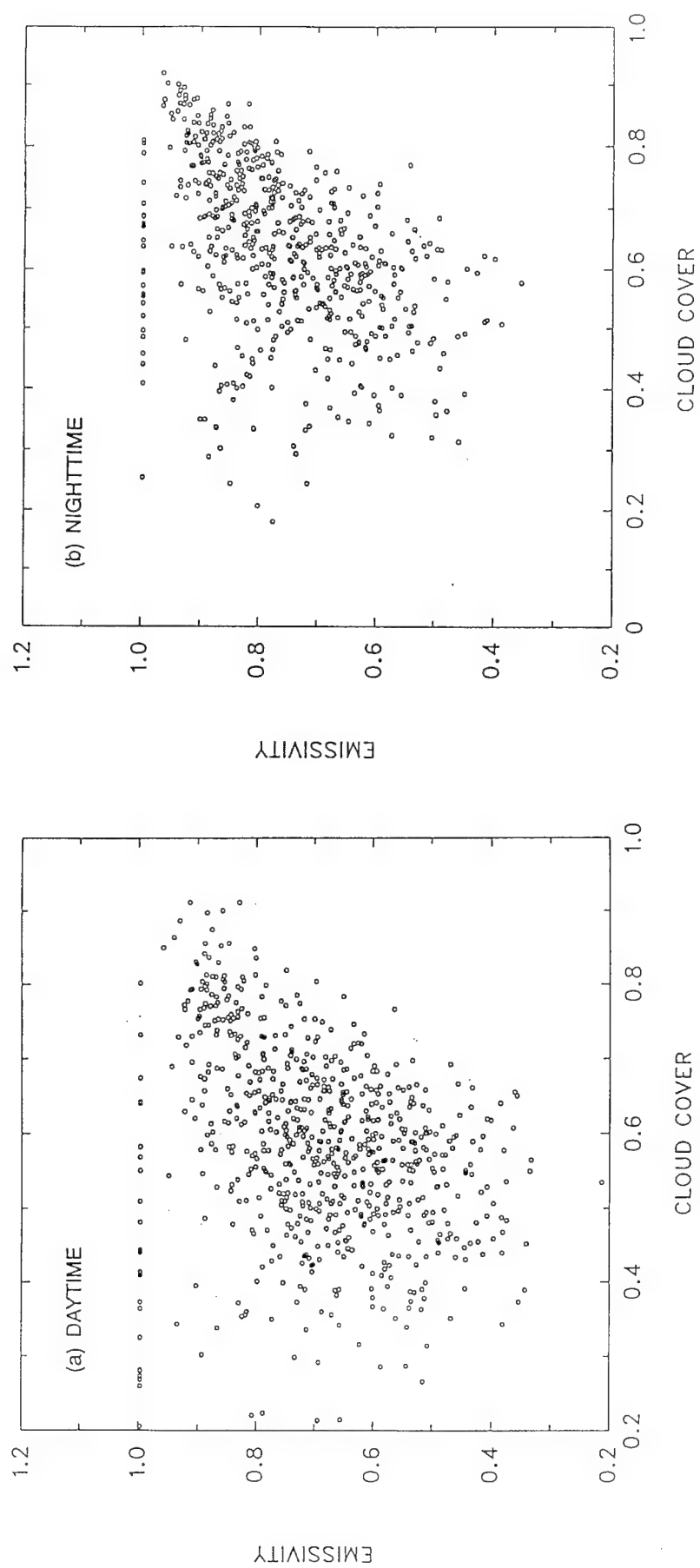
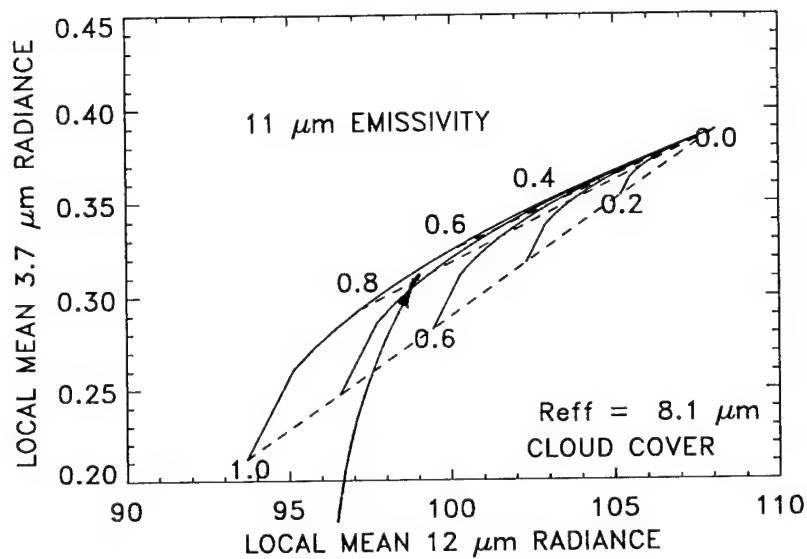


Figure 6

Bispectral Consistency

12-3.7 μm



11-12 μm

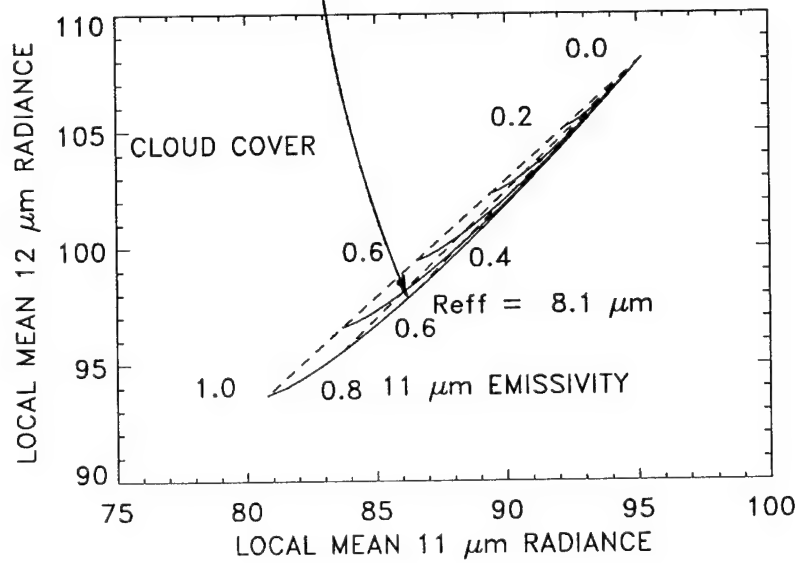
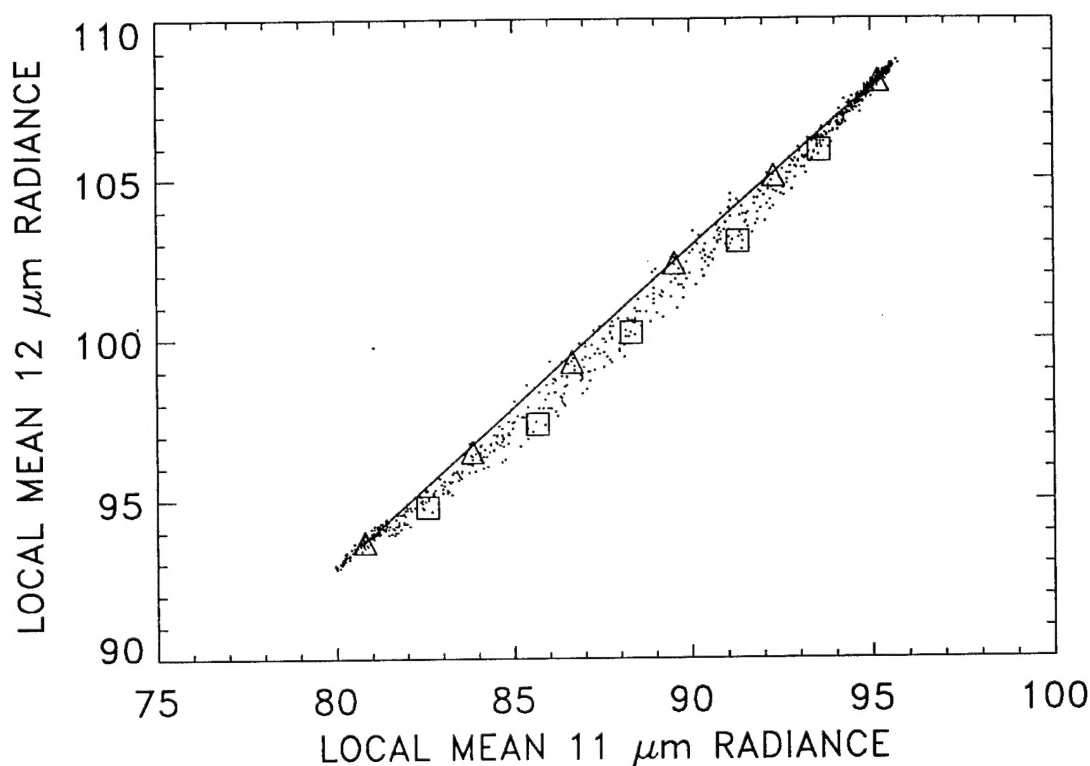


Figure 7

Pixel Cluster Locations in the Multispectral Radiance Domain

11–12 μm Radiance Pairs



Triangles—pixels containing opaque, broken cloud.

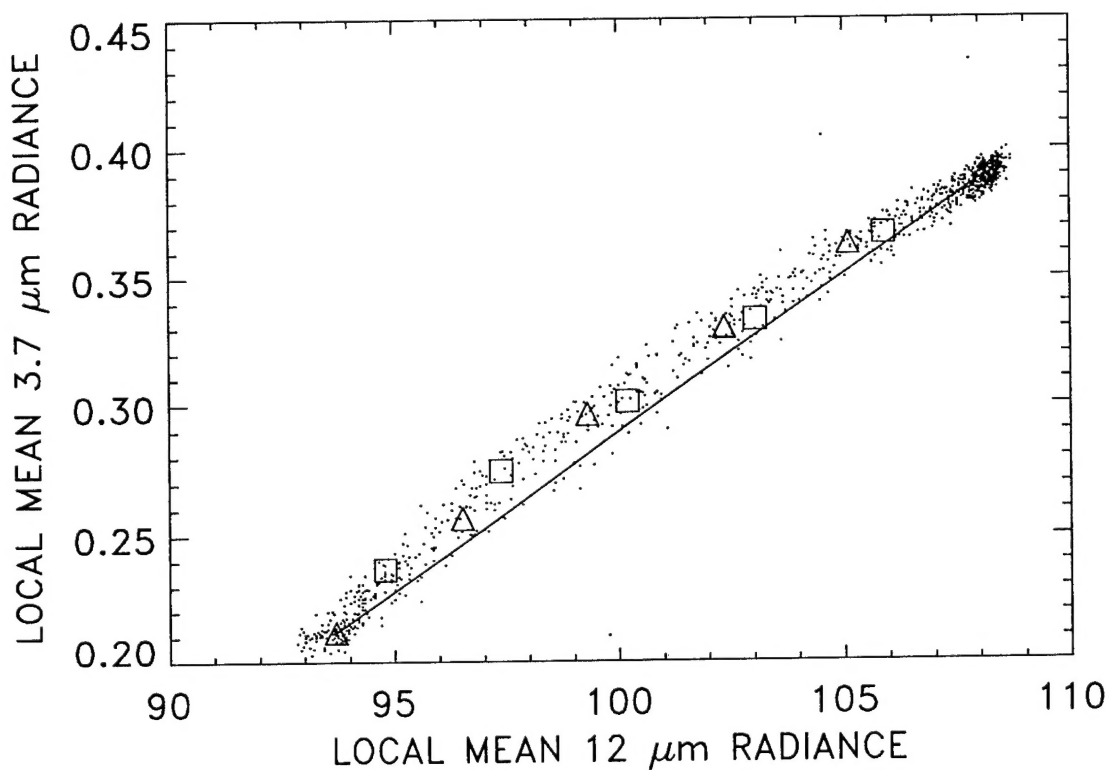
Squares—pixels overcast by semitransparent cloud

2 × 2 arrays of 1-km HRPT data from nighttime overpass of NOAA-11 for 60-km scale portion of ASTEX region containing single-layered marine stratocumulus system. 10 June 1992, 0412 Z

Figure 8

Pixel Cluster Locations in the Multispectral Radiance Domain

12–3.7 μm Radiance Pairs



Triangles—pixels containing opaque, broken cloud.

Squares—pixels overcast by semitransparent cloud

2 × 2 arrays of 1-km HRPT data from nighttime overpass of NOAA-11 for 60-km scale portion of ASTEX region containing single-layered marine stratocumulus system. 10 June 1992, 0412 Z

Figure 9

Ceilometer vs. Coakley cloud amount correlation

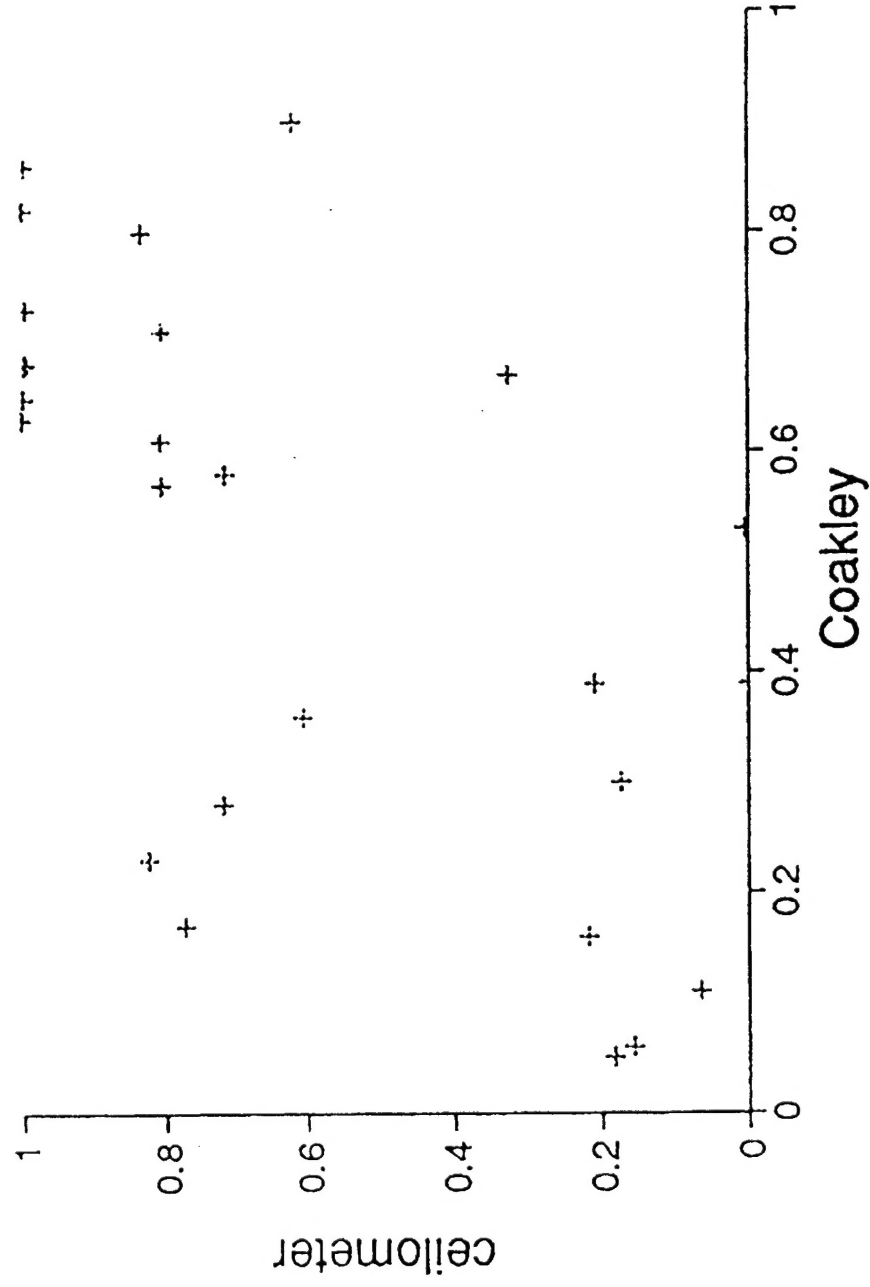


Figure 10

Porto Santo low cloud:
ECMWF vs. 3 hr avg ceilometer cloud amount correlation

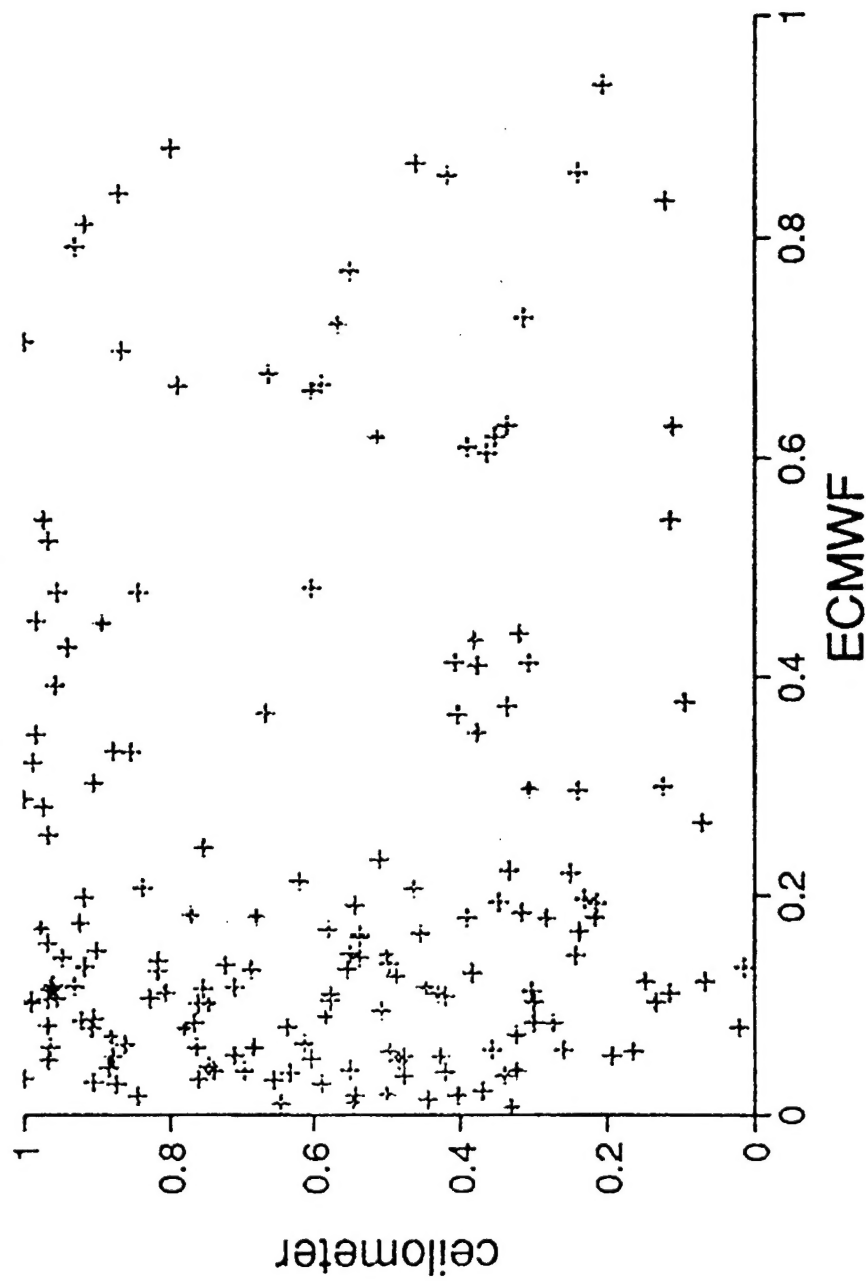


Figure 11